SUPPORTING INFORMATION

A potent candidate against Zika virus infection: Synthesis, bioactivity, radiolabeling and biodistribution studies

Sumit Kumar[1,#], Neha Sharma[2,#], Willyenne Dantas[3], Jessica Catarine Frutuoso do Nascimento[3], Hannah Maus[4], Ronaldo Nascimento de Oliveira[5], Unnat Pandit[6], Agam, P Singh[7], Tanja Schirmeister[4], Puja Panwar Hazari[8], Lindomar Pena[3], Poonam[1,9]*, Brijesh Rathi[2,9]*

[1]*Department of Chemistry, Miranda House, University of Delhi, Delhi – 110007 India*
[2]*Har Gobind Khorana Centre For Chemical Biology, Department of Chemistry, Hansraj College, University of Delhi, Delhi – 110007 India*
[3]*Department of Virology, Aggeu Magalhaes, Institute (IAM), Oswaldo Cruz Foundation (Fiocruz), Recife 50670-420, Pernambuco, Brazil*
[4]*Institute of Pharmaceutical and Biomedical Sciences, Johannes Gutenberg University, 55128 Mainz, Germany*
[5]*Department of Chemistry, Federal Rural University of Pernambuco, Dois Irm~aos, 52171-900, Recife, Brazil*
[6]*Special Centre for Systems Medicine, Jawaharlal Nehru University, New Delhi 110067, India*
[7]*Infectious Diseases Laboratory, National Institute of Immunology, New Delhi 110067, India*
[8]*Division of Cyclotron and Radiopharmaceutical Sciences Institute of Nuclear Medicine and Allied Sciences, New Delhi 110054, India*
[9]*Delhi School of Public Health, Institution of Eminence, University of Delhi, Delhi-110007*

#Both the authors contributed equally

*Corresponding Author:

Poonam, M.Phil., Ph.D.

poonam.chemistry@mirandahouse.ac.in

ORCID: 0000-0002-3759-1057

Brijesh Rathi, PhD

brijeshrathi@hrc.du.ac.in

ORCID: 0000-0003-2133-8847

SUPPORTING INFORMATION

Table of Content:

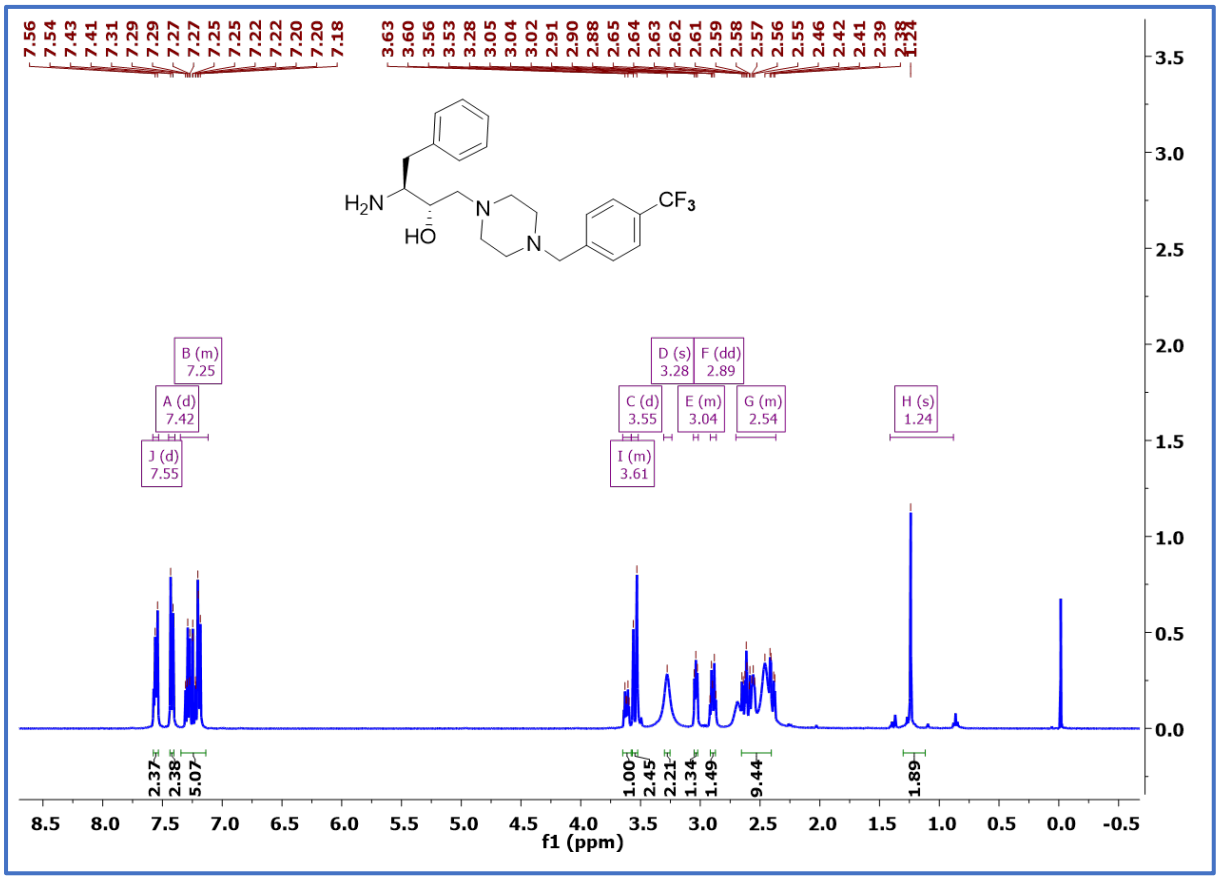

Figure S1. ^{1}H NMR data of compound, **VI** in $CDCl_3$.

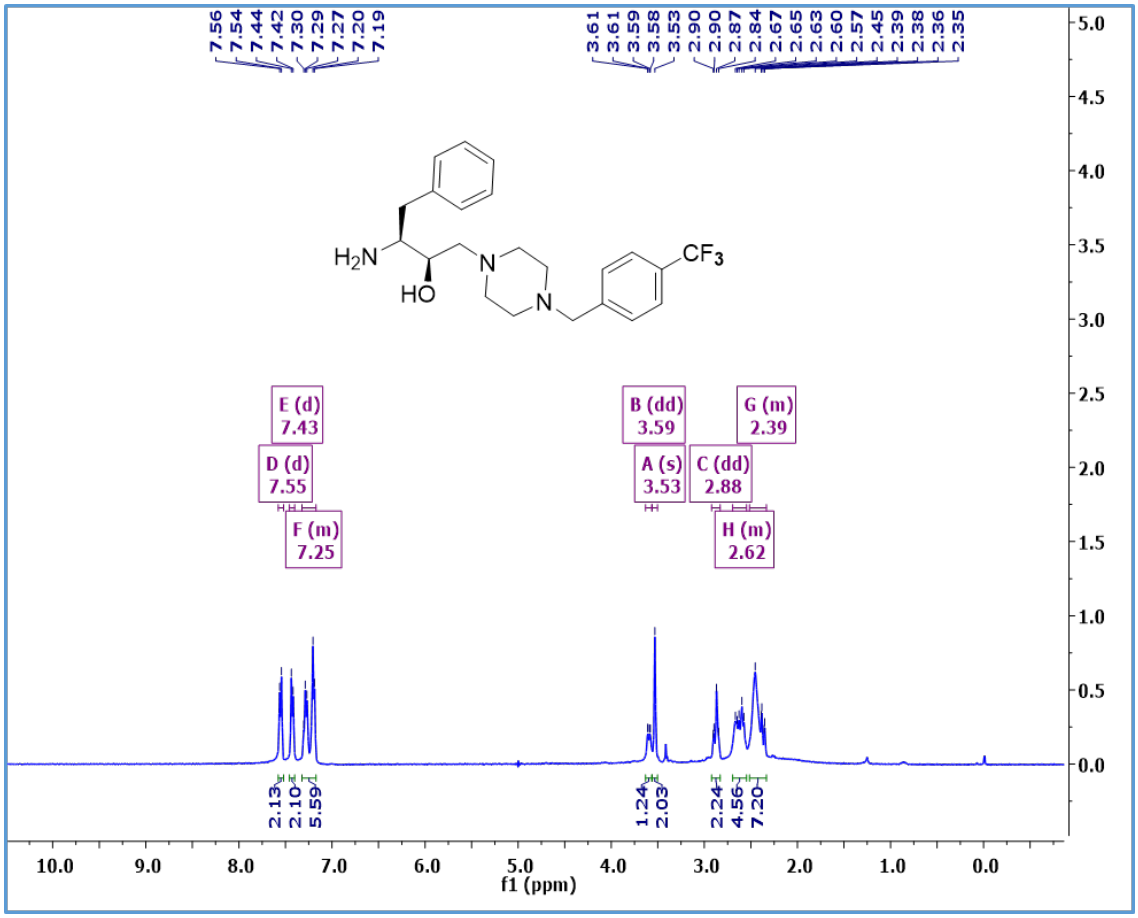

Figure S2. ^{1}H NMR data of compound, **VII** in $CDCl_3$.

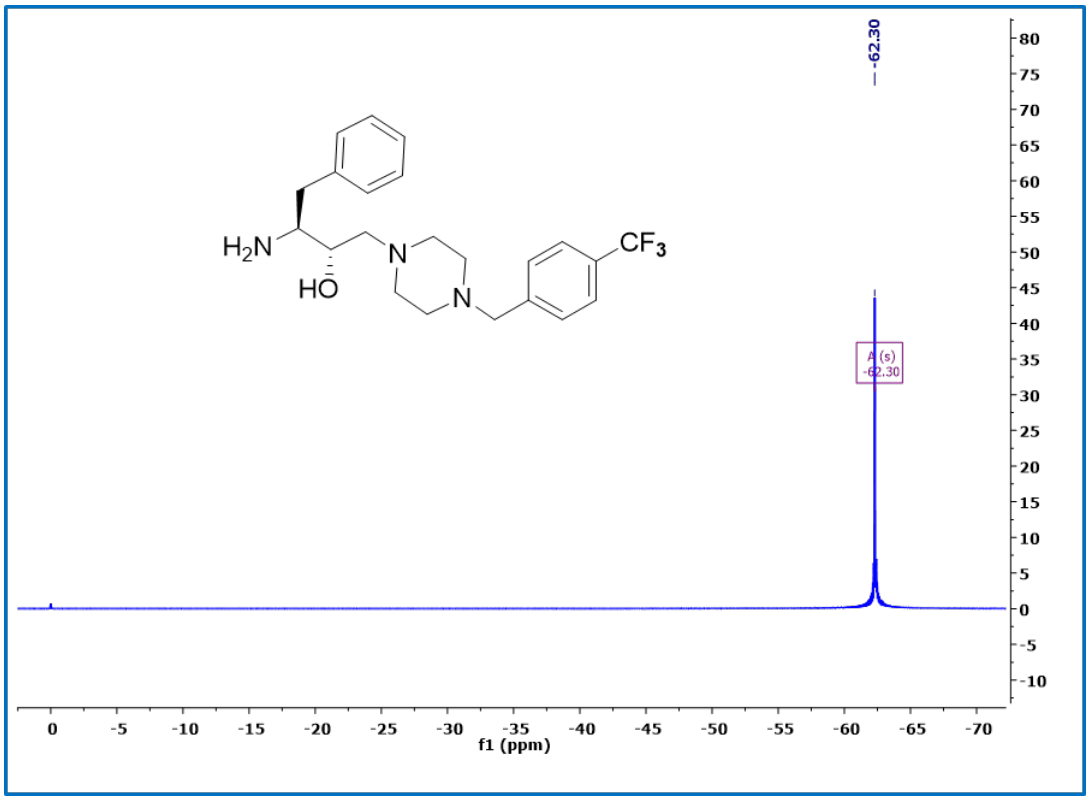

Figure S3. ^{19}F NMR data of compound, **VI** in $CDCl_3$.

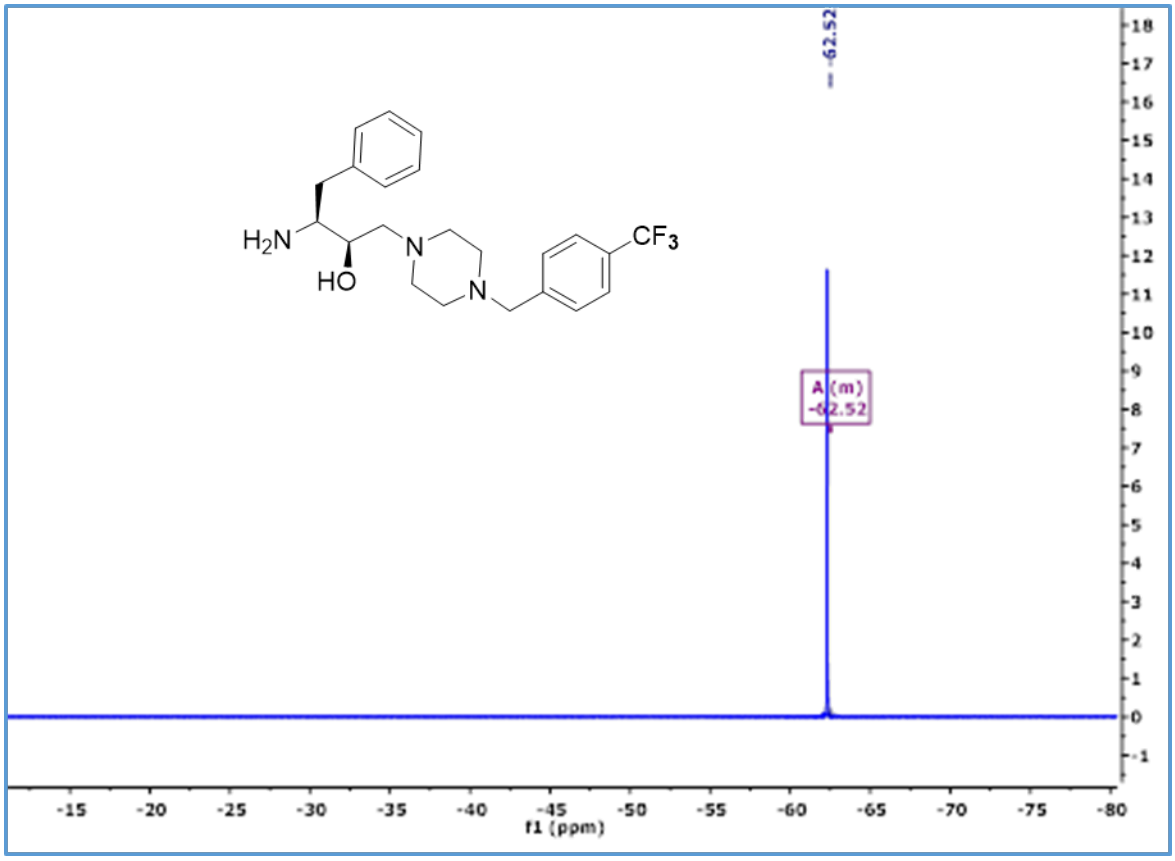

Figure S4. ^{19}F NMR data of compound, **VII** in $CDCl_3$.

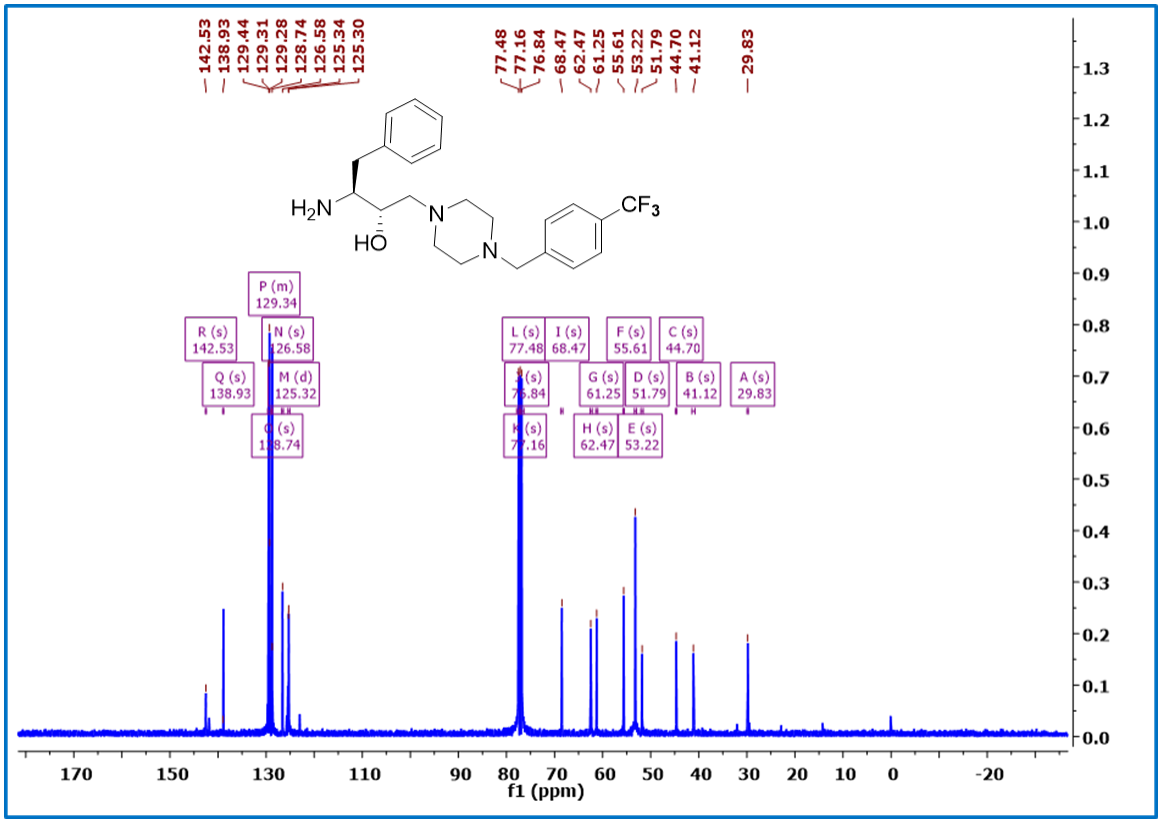

Figure S5. ^{13}C NMR data of compound, **VI** in $CDCl_3$.

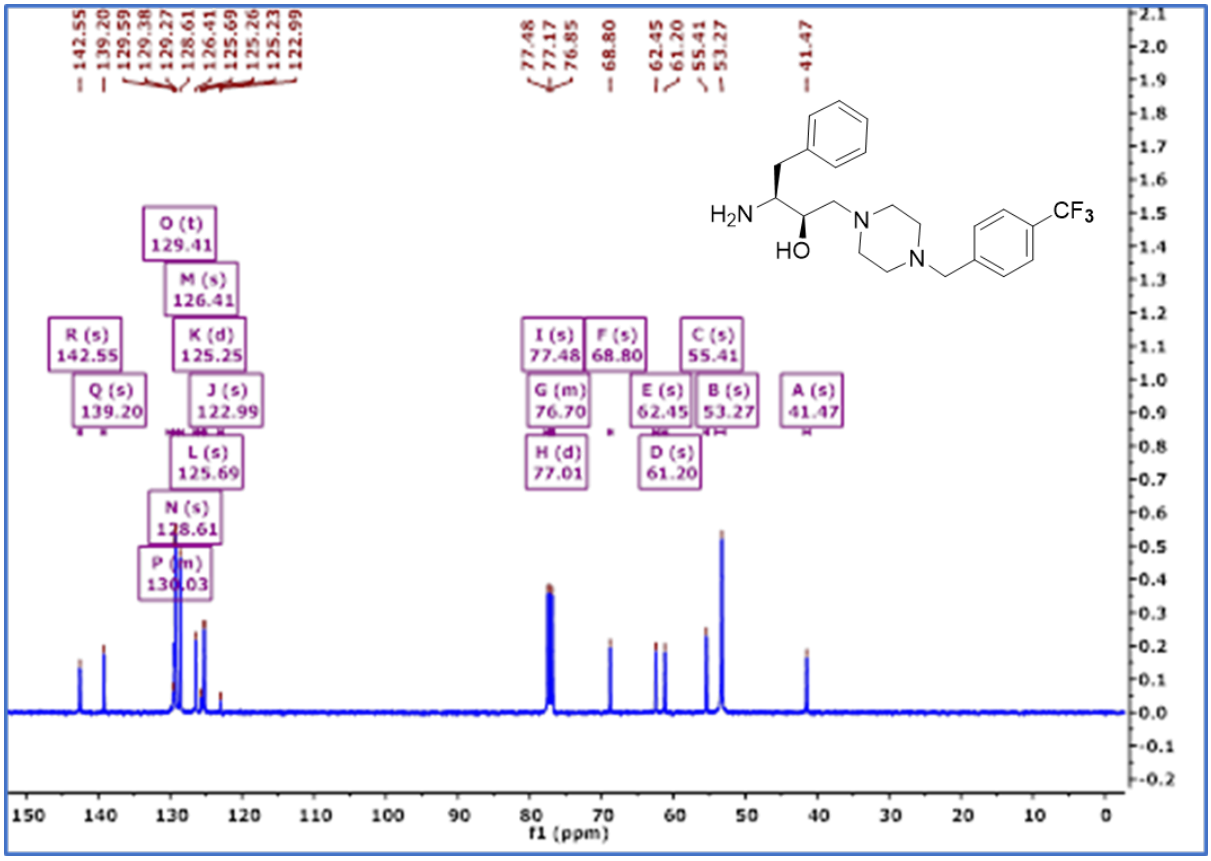

Figure S6. ^{13}C NMR data of compound, **VII** in $CDCl_3$.

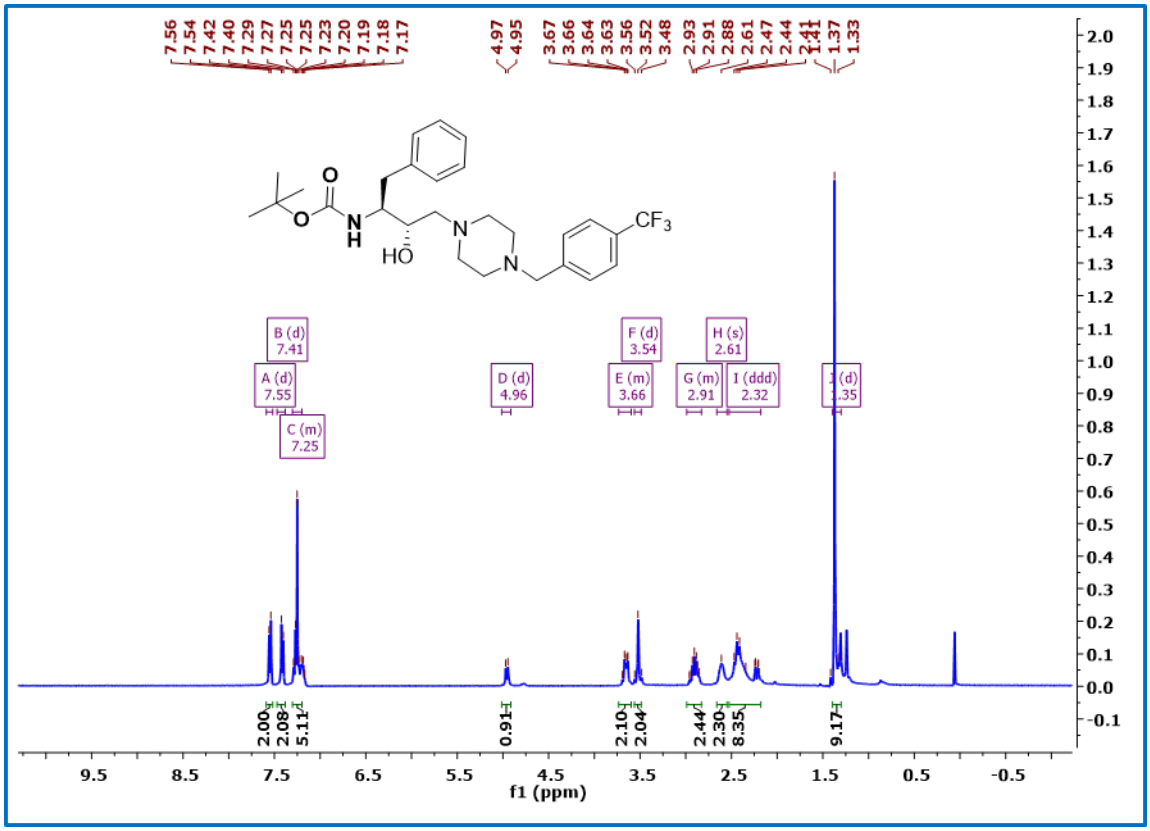

Figure S7. ^{1}H NMR data of compound, **IV** in $CDCl_3$.

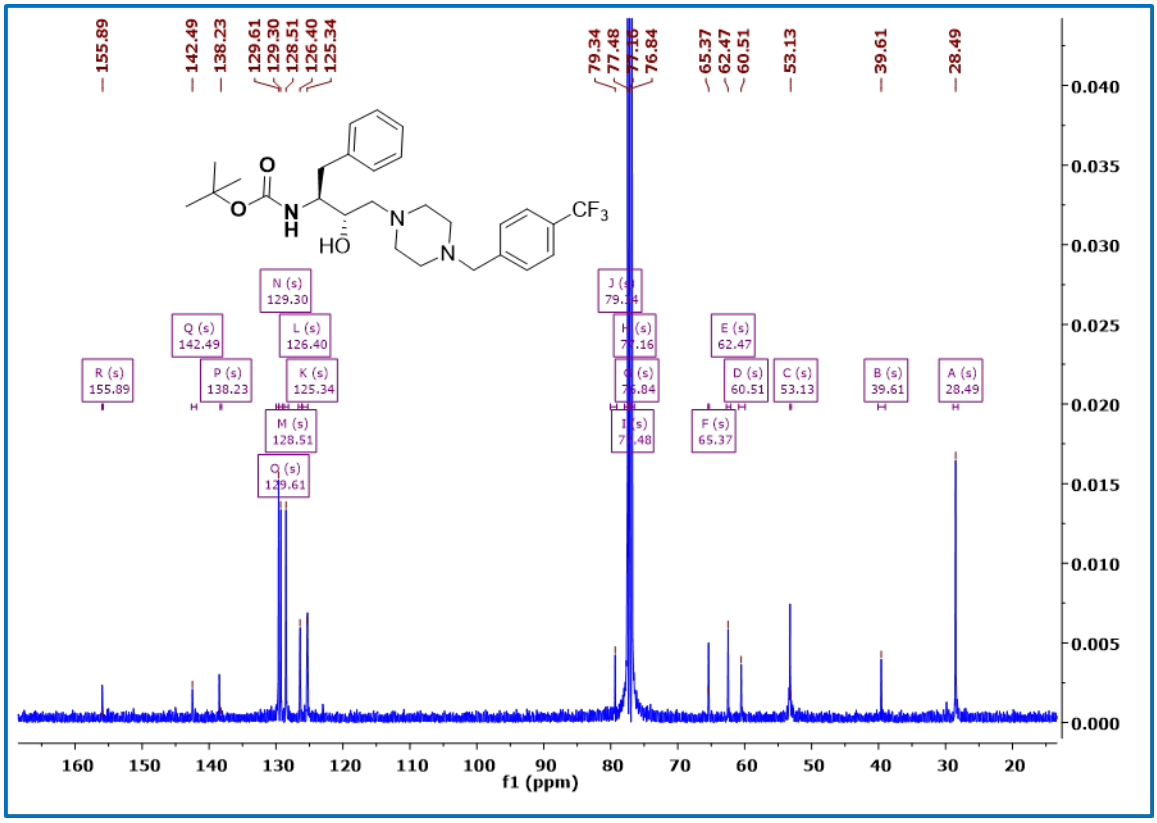

Figure S8. ^{13}C NMR data of compound, **IV** in $CDCl_3$.

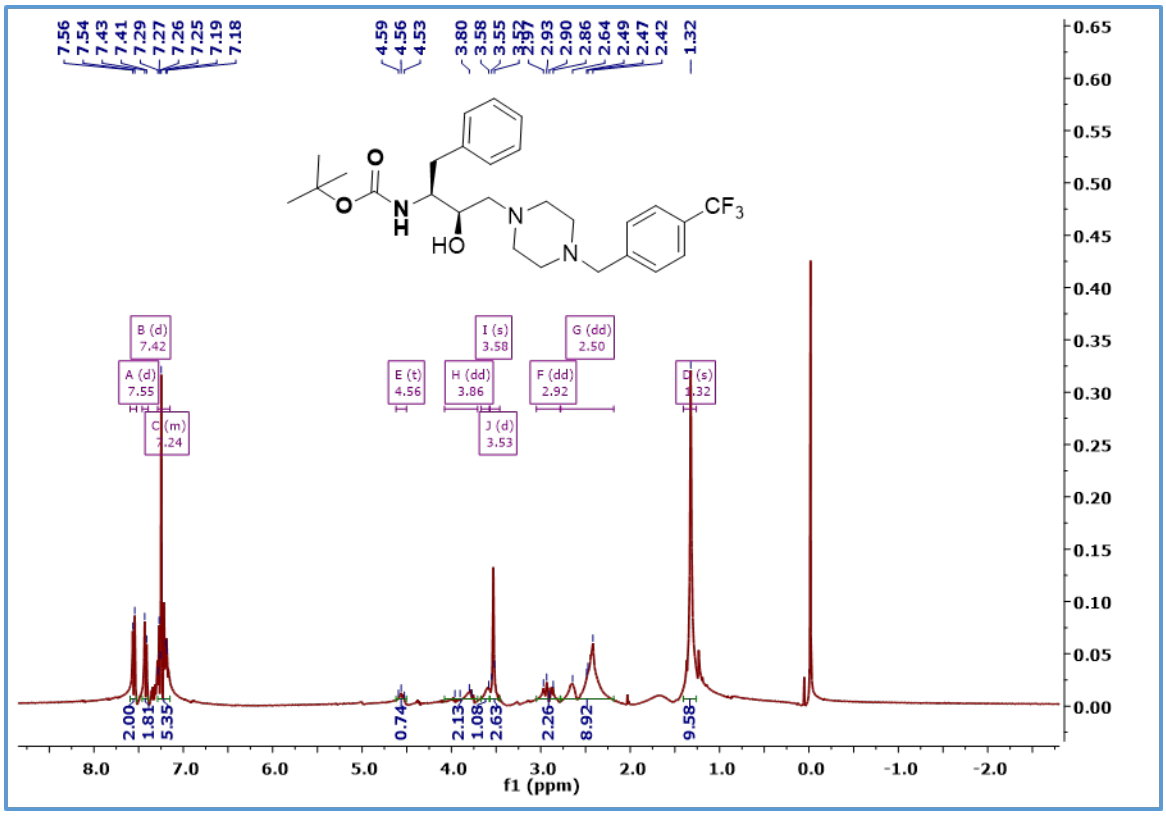

Figure S9. ^{1}H NMR data of compound, **V** in $CDCl_3$.

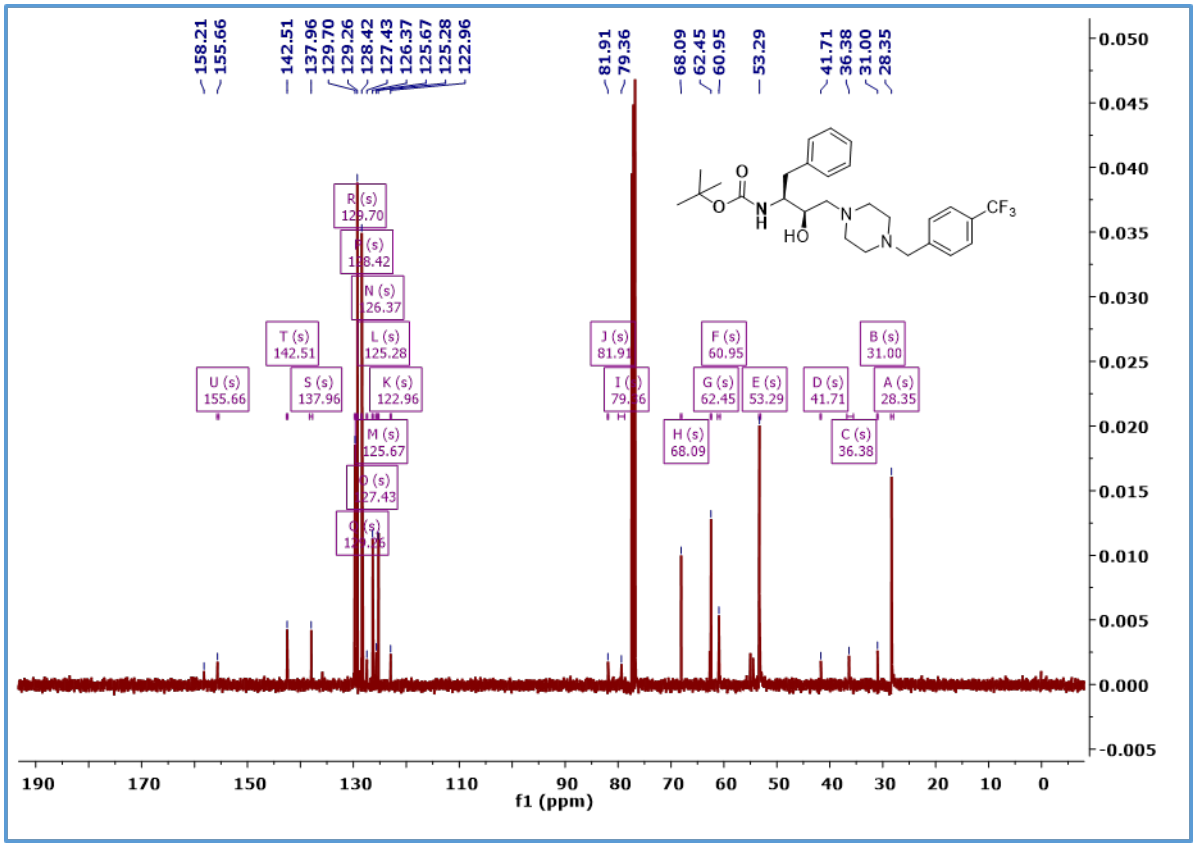

Figure S10. ^{13}C NMR data of compound, **V** in $CDCl_3$.

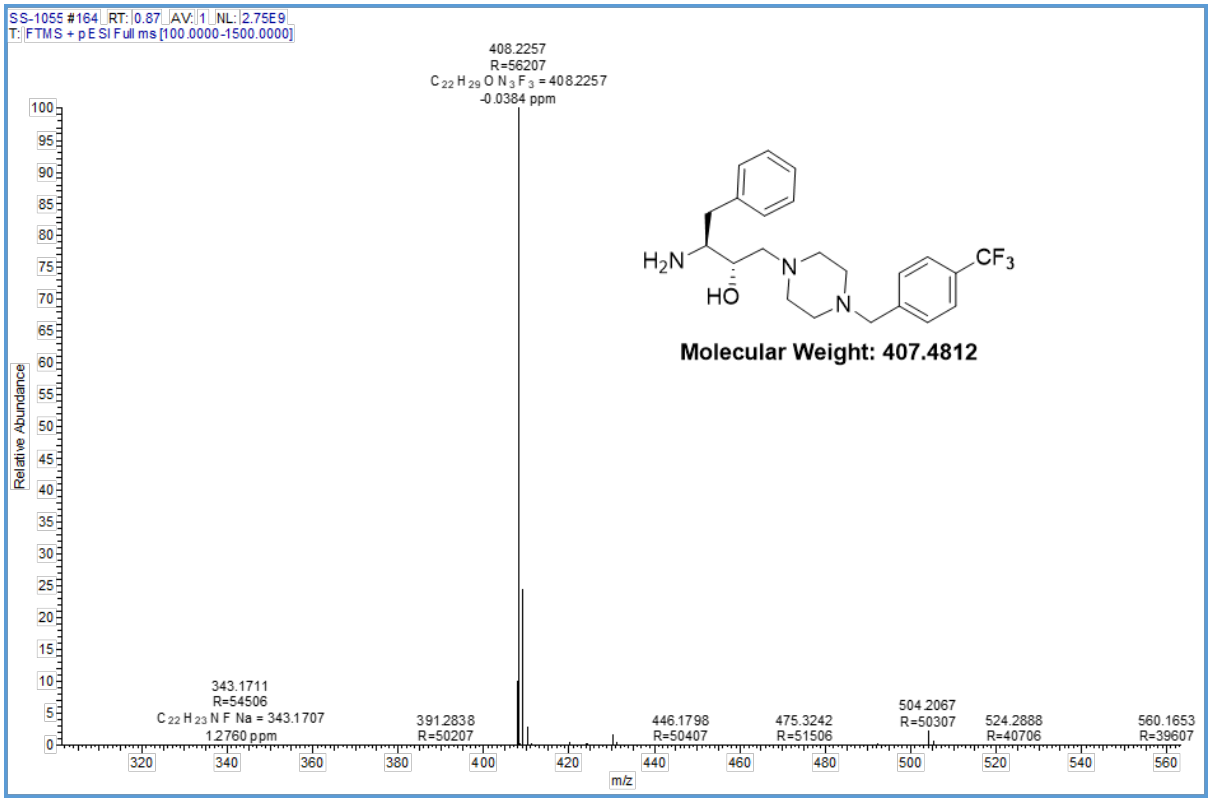

Figure S11. ESI (HR-MS) spectrum of **VI**.

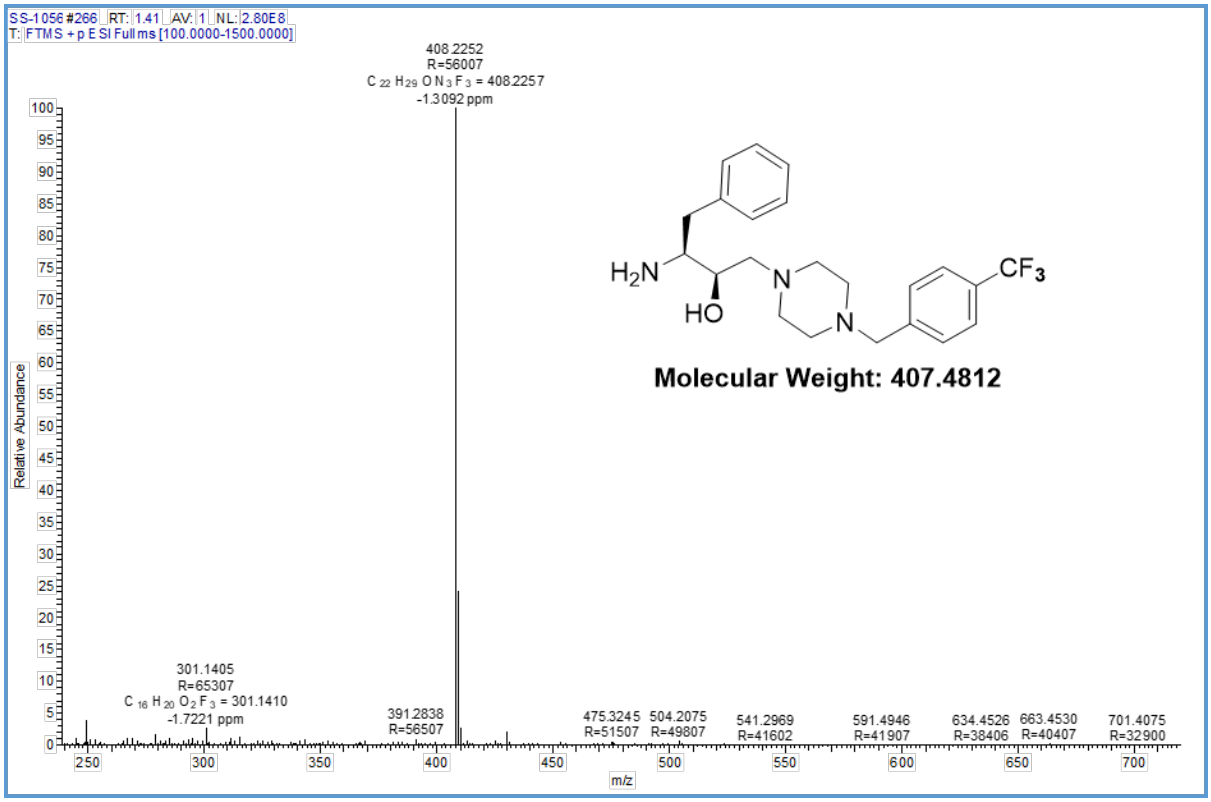

Figure S12. ESI (HR-MS) spectrum of **VII**.

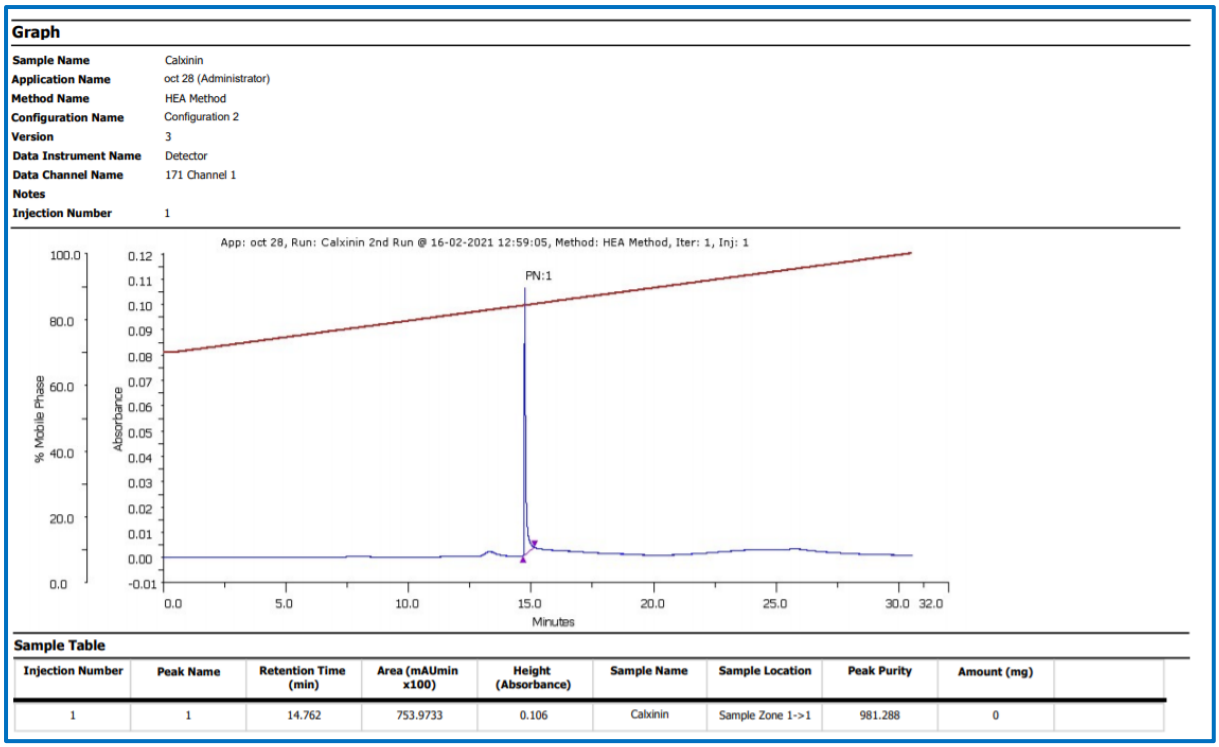

Figure S13. HPLC purity analysis for first cycle of **VI**.

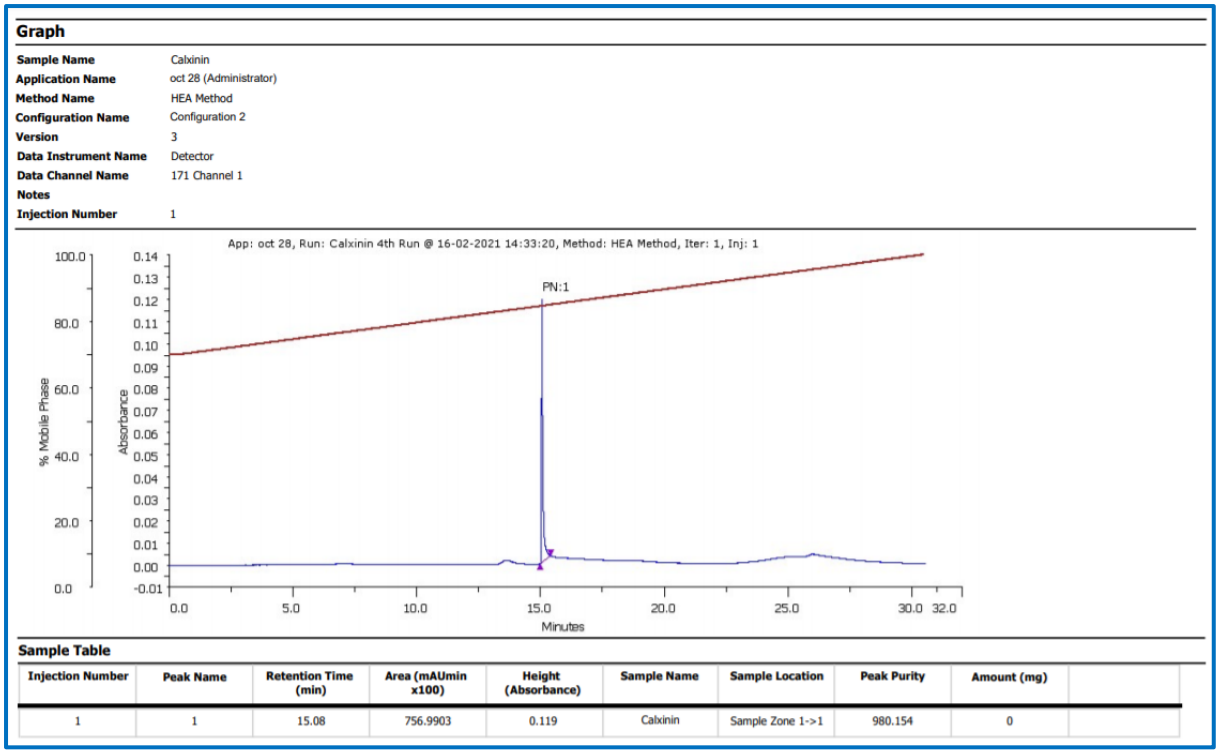

Figure S14. HPLC purity analysis for second cycle of **VI**.

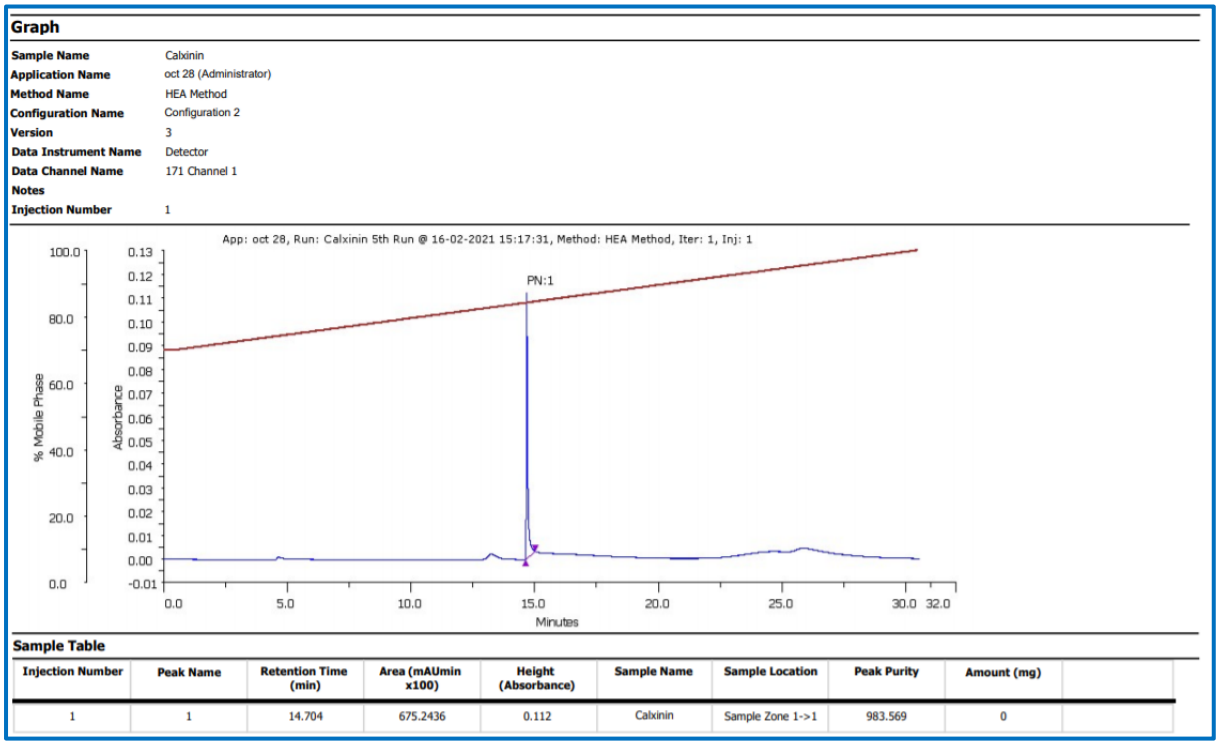

Figure S15. HPLC purity analysis for third cycle of **VI**.

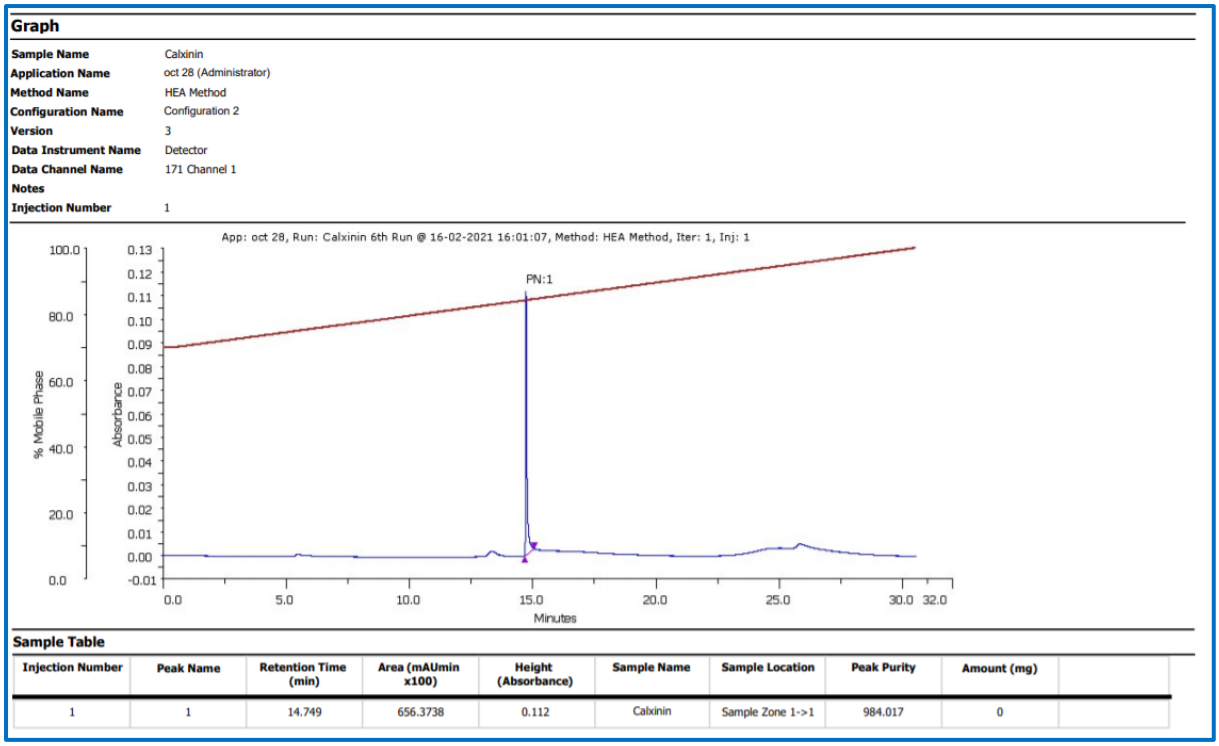

Figure S16. HPLC purity analysis for fourth cycle of **VI**.

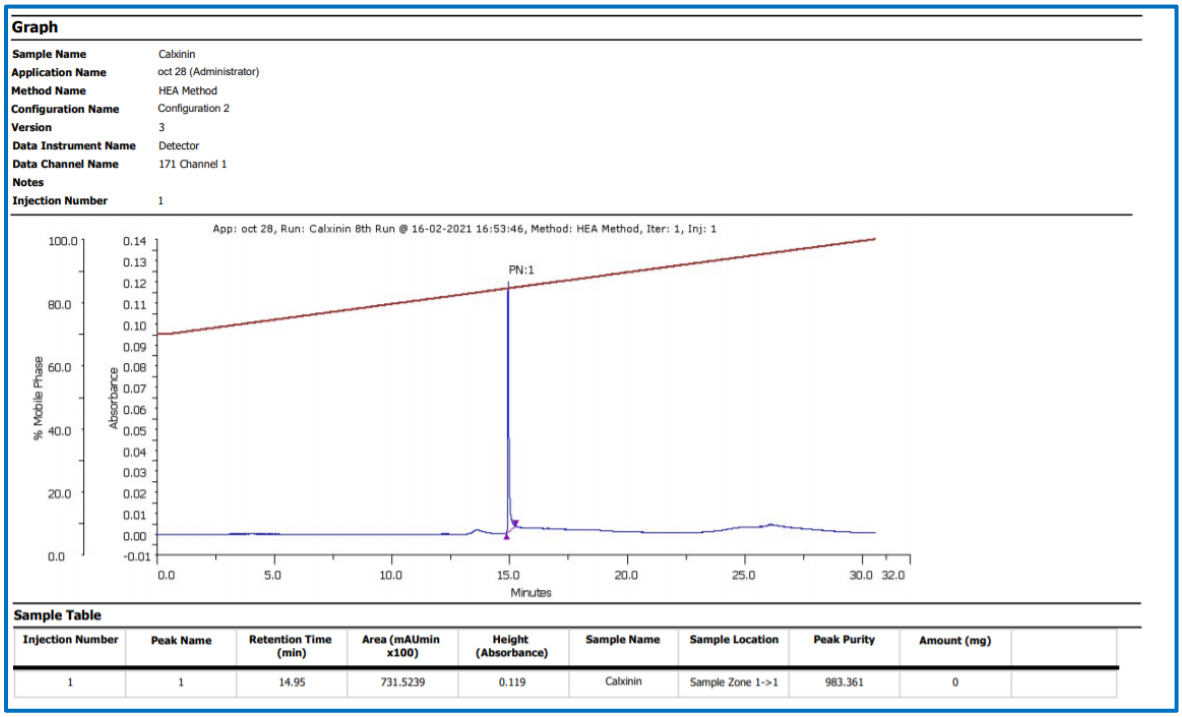

Figure S17. HPLC purity analysis for fifth cycle of **VI**.

Table S1. Average peak purity and retention time of **VI** after five successive HPLC analysis with a flow 0.3 mL/min started at 70:30:0.01 (acetonitrile:water:TFA) to 100:0:0.01 and a total run time of 30 min.

Entry No.	Peak Purity (%)	Retention Time (min.)
1.	98.1	14.76
2.	98.0	15.08
3.	98.3	14.70
4.	98.4	14.75
5.	98.3	14.95
Average	**98.2**	**14.84**

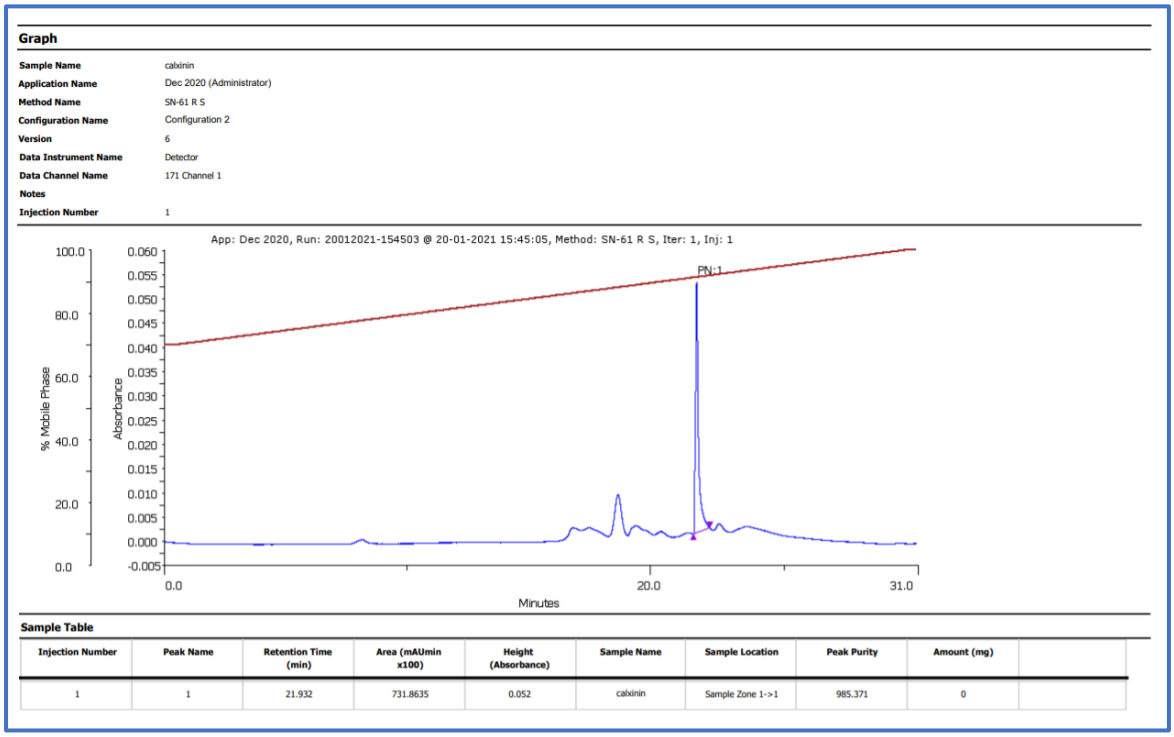

Figure S18. HPLC purity analysis of compound **VII**.

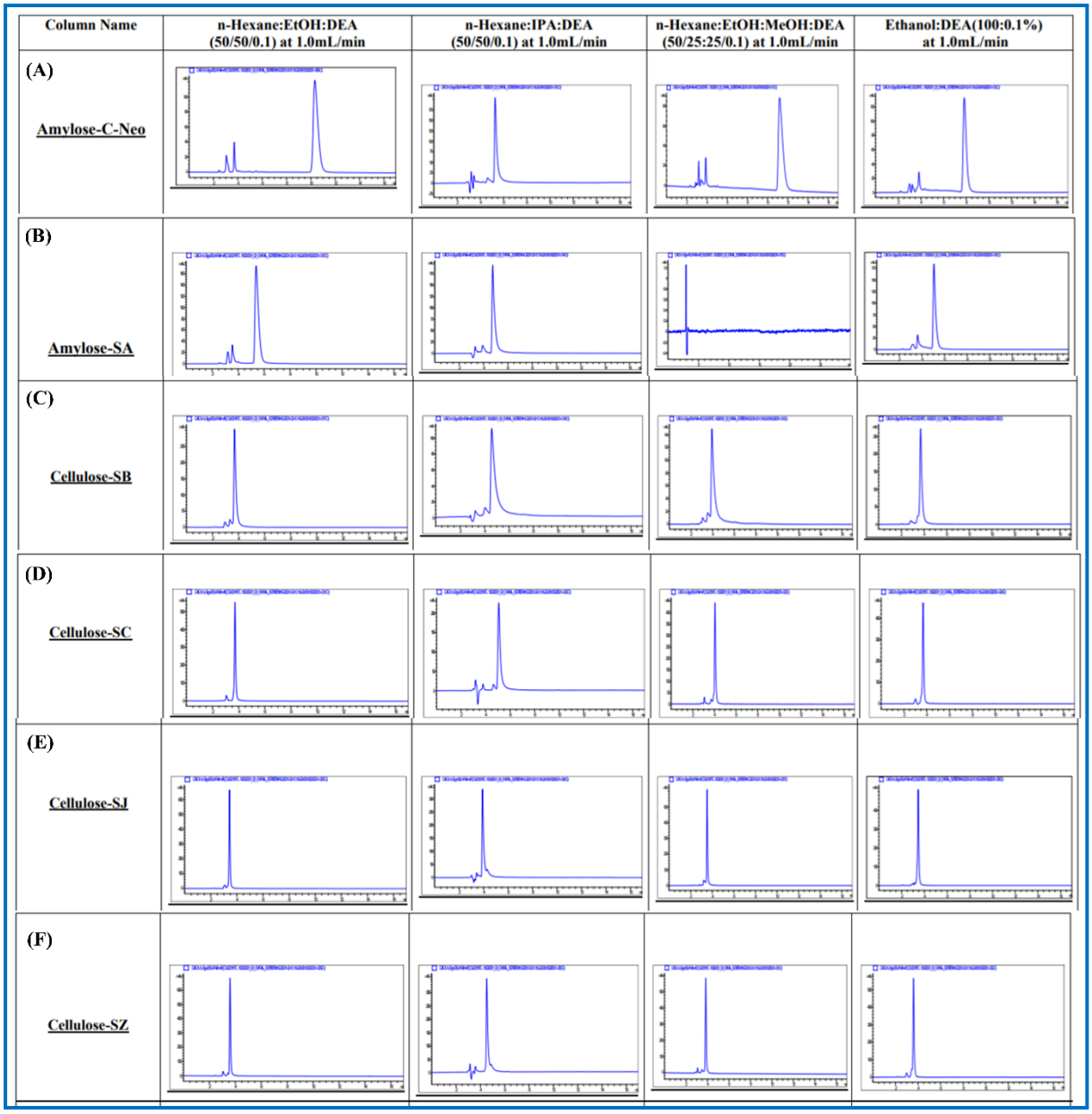

Figure S19. HPLC analysis for compound **VI** using four different non-polar solvent systems (n-hexane:EtoH:DEA (50:50:0.1), n-hexane:IPA:DEA (50:50:0.1), n-hexane:EtOH:MeOH:DEA (50:25:25:0.1), and EtOH:DEA (100:0.1)) at flow rate of 1.0 mL/min for a run time of 15 min with six chiral columns which are: (A) Amylose-C-Neo; (B) Amylose-SA; (C) Cellulose-SB; (D) Cellulose-SC; (E) Cellulose-SJ; and (F) Cellulose-SZ.

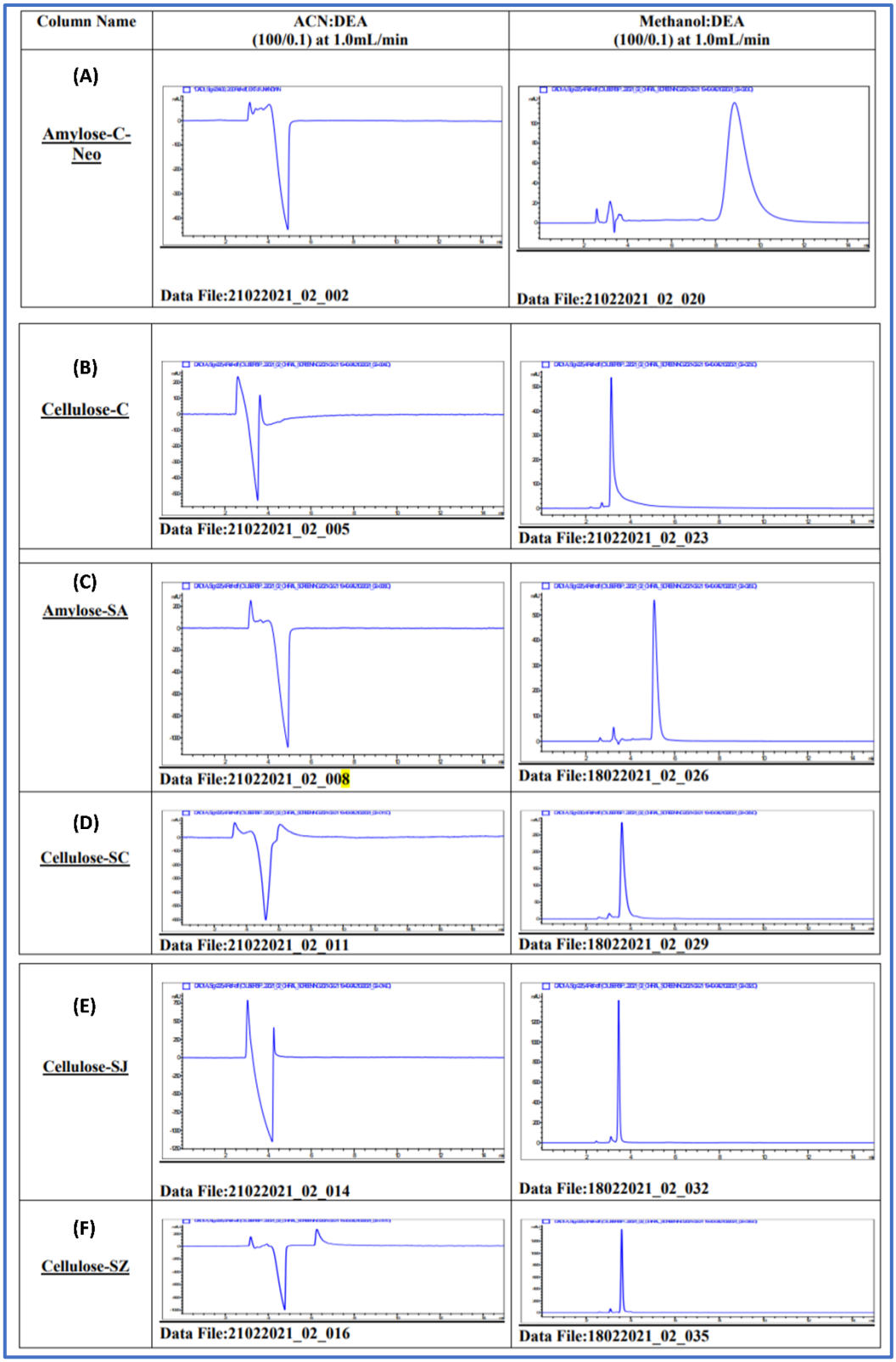

Figure S20. HPLC analysis of compound **VI** using two different polar solvent systems (ACN:DEA (100:0.1) and Methanol:DEA (100:0.1) at flow rate of 1.0 mL/min for a run time of 15 min with six chiral columns which are: (A) Amylose-C-Neo; (B) Amylose-SA; (C) Cellulose-SB; (D) Cellulose-SC; (E) Cellulose-SJ; and (F) Cellulose-SZ.

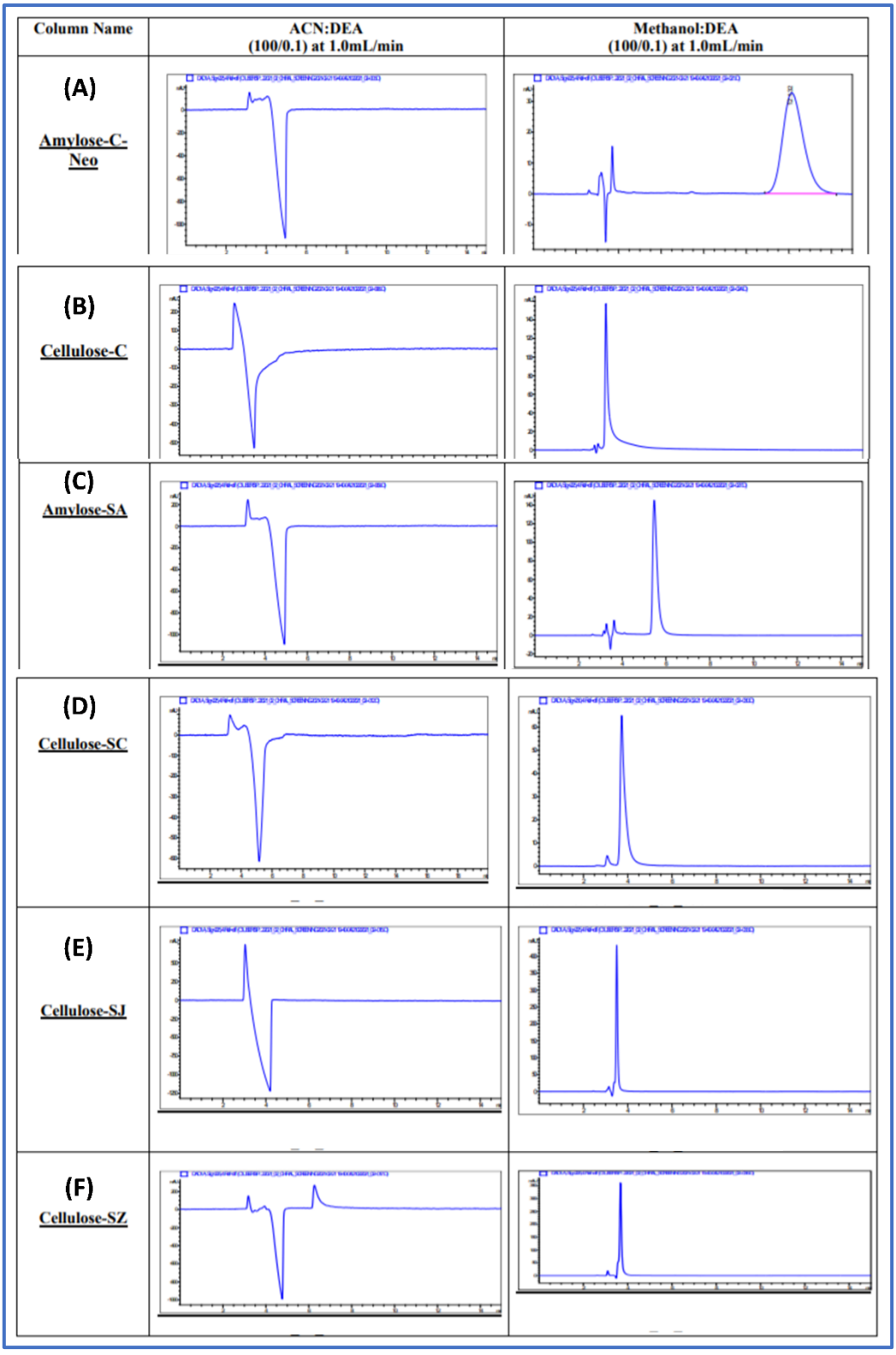

Figure S21. HPLC analysis of compound **VII** using two different polar solvent systems (ACN:DEA (100:0.1) and Methanol:DEA (100:0.1) at flow rate of 1.0 mL/min for a run time of 15 min with six chiral columns which are: (A) Amylose-C-Neo; (B) Amylose-SA; (C) Cellulose-SB; (D) Cellulose-SC; (E) Cellulose-SJ; and (F) Cellulose-SZ.

Table S2. The molecular docking results for compound **VI**, with all three targeted proteins.

Entry No.	Protein	Docking Score in Kcal/mol	XP Gscore in Kcal/mol	MMGBSA (ΔG) in Kcal/mol
1.	Helicase	-2.381	-3.065	-38.15
2.	Protease	-6.039	-6.857	-44.53
3.	Methyltransferase	-4.027	-4.711	-49.67

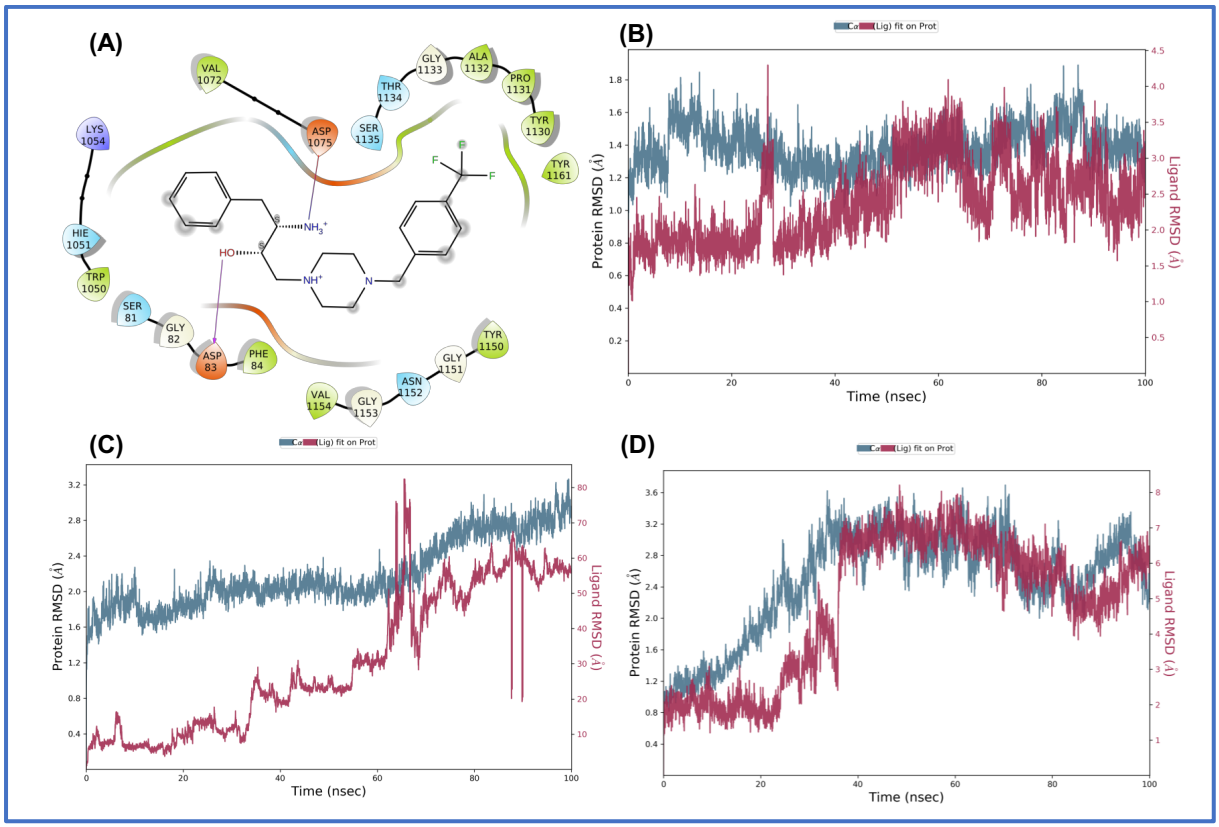

Figure S22. Schematic representation of 2D interaction maps against protease enzyme of ZIKV infection. A) compound **VI** (identified potent analog). Root mean square deviations (RMSD) difference between the proteins of ZIKV infections and bound ligand **VI** during 100 ns MD simulation. B) compound **VI**-protease complex; C) compound **VI**-helicase complex; and D) compound **VI**-methyltransferase complex. The graph was obtained for the RMSD value of ligand (brown line) from the protein backbone (blue line). The compound **VI**-protease complex quickly stabilized to a very low energy state (within 25 ns) and was highly stable throughout the simulation.

Table S3. Biodistribution of ^{99m}Tc-**VI** in different parts following intravenous injection in Strain-A (20-22g) mice at different time intervals (1h, 2h, 4h, and 24h). The data was compiled for accumulated amount (% ID/g = % injected dose per gram).

	1h		2h		4h		24h	
Organ	%ID/g	Std. Dev.	%ID/g	Std. Dev.	%ID/g	Std. Dev.	%ID/g	Std. Dev.
Blood	0.015766	0.001183	0.041195	0.018306	0.03415	0.015344	0.002116	0.000827
Heart	0.048525	0.024040	0.042936	0.024344	0.036391	0.027395	0.006355	0.002483
Lungs	0.070367	0.074480	0.048432	0.034486	0.100061	0.063476	0.012828	0.005013
Liver	1.239575	0.025000	0.756882	0.019798	0.396096	0.172023	0.131663	0.051451
Spleen	0.045015	0.001877	0.048843	0.023902	0.045241	0.042199	0.061509	0.024037
Kidney	1.326025	0.014000	0.783219	0.018000	0.735649	0.023000	0.203914	0.079686
Stomach	0.026136	0.013340	0.028316	0.019614	0.024178	0.024476	0.005165	0.006521
Brain	0.094422	0.086989	0.141614	0.128695	0.128198	0.150255	0.011689	0.014757
Muscle	0.039236	0.001966	0.047576	0.029294	0.03047	0.025978	0.040164	0.015696
Intestine	0.29434	0.063365	0.243789	0.010000	0.152077	0.015855	0.010414	0.004069
Bone	0.003382	0.002073	0.025825	0.004256	0.004165	0.001438	0.006311	0.002466
Lung/Blood	4.4644	-	1.1756	-	2.9300	-	6.0723	-
Lungs/Muscle	1.7937	-	1.0198	-	3.283	-	3.1942	-
Brain/Blood	6.012	-	3.44	-	3.76	-	5.844	-

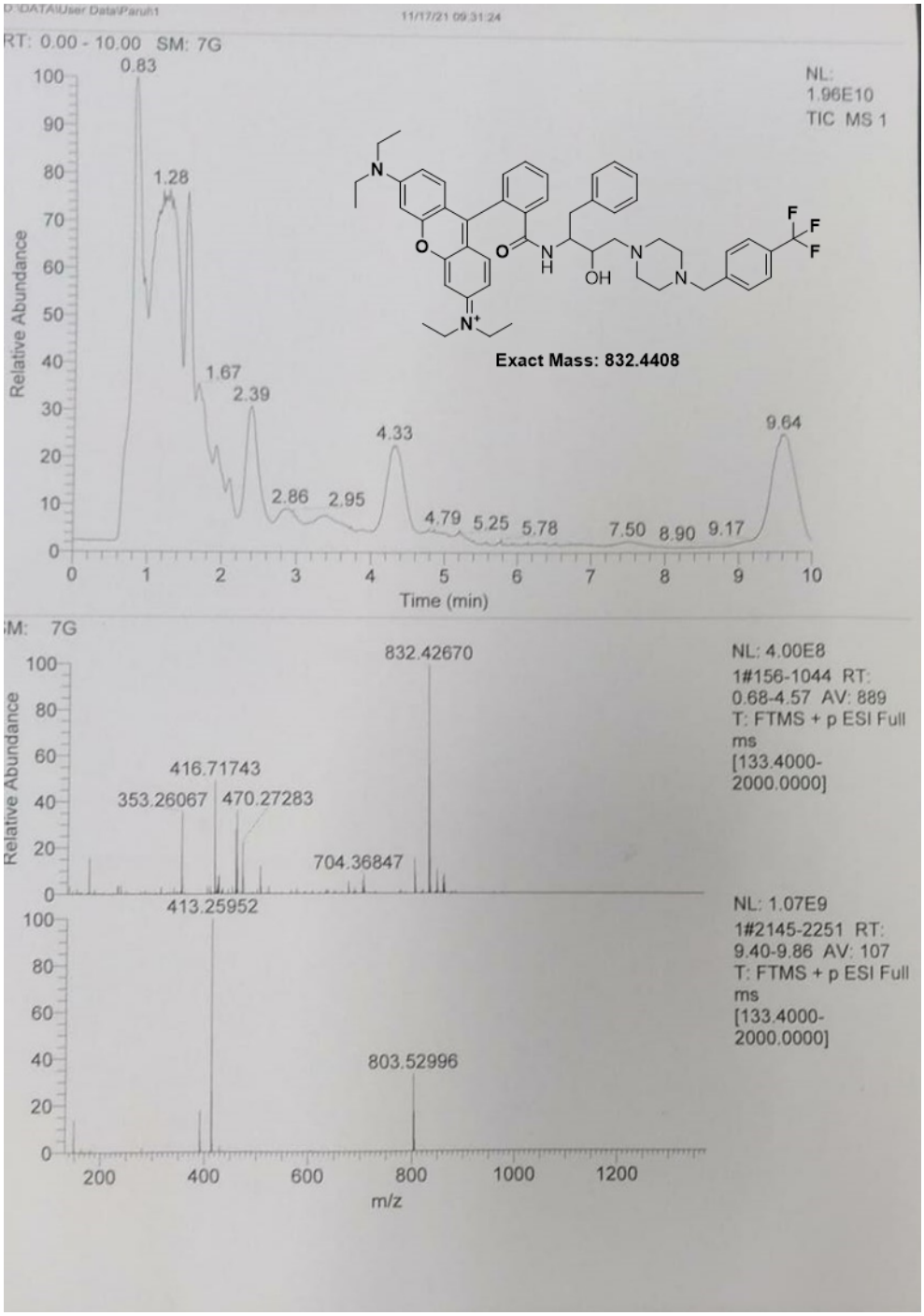

Figure S23. High-resolution mass spectroscopy (HRMS) spectra of Rhodamine b (Rho) conjugated compound (**VI**) indicated the formation of complex with characteristics mass peak at 832.42670 (expected peak: 832.4408).

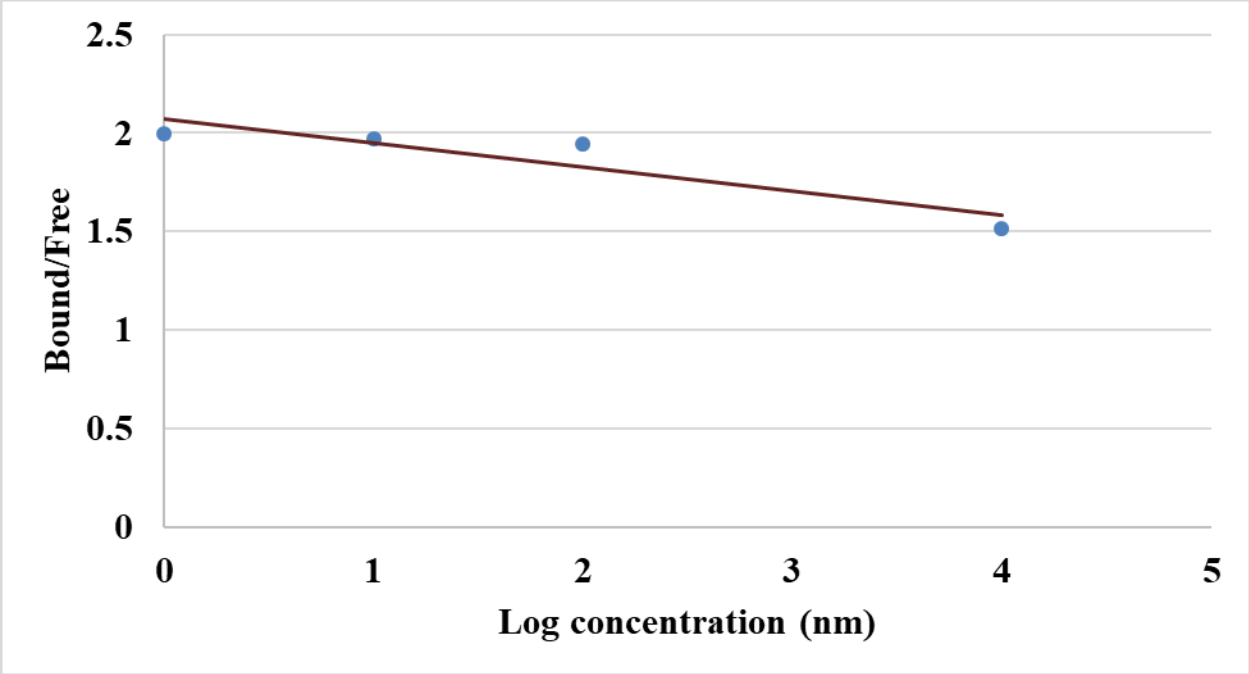

Figure S24. Saturation curve obtained from radioligand binding affinity experiment of the hippocampus of rat brain. Non-specific binding was determined with a 100-fold concentration of Rho-VI complex, where K_d of 7.54 nM was obtained for the 5-HT1A receptor.

Preparation of VI–rhenium (Re) adduct.

Reports are available stating the similar coordination chemistry of Re and ^{99m}Tc.[1] Therefore, Re as an analogue of Tc could be used as a useful tool to direct studies toward radioactive ^{99m}Tc adduct. We have adopted the same methodology to establish the structure of radiolabeled **VI** using Re(III)chloride, [Re(III)Cl_3]. The surrogate Re adduct of ^{99m}Tc-**VI** was prepared. Equimolar concentrations of Re(III) chloride (4.6 mg; 16.05 µmol) and 5 mg (16.05 µmol) of the unlabeled compound **VI** were dissolved in 0.5 M sodium hydroxide (1 mL). The reaction mixture was then heated at 90 °C for 1 hour under basic conditions (~14 pH). We observed a clear change from blackish-brown to the transparent solution. The crude reaction mixture of Re–**VI** adduct was characterized from High Resolution Mass Spectroscopy (HRMS) as shown in Figure S25. In the HRMS, the calculated and observed mass values indicated the formation of the plausible 1:1 adduct of Re–**VI** (Table S4).

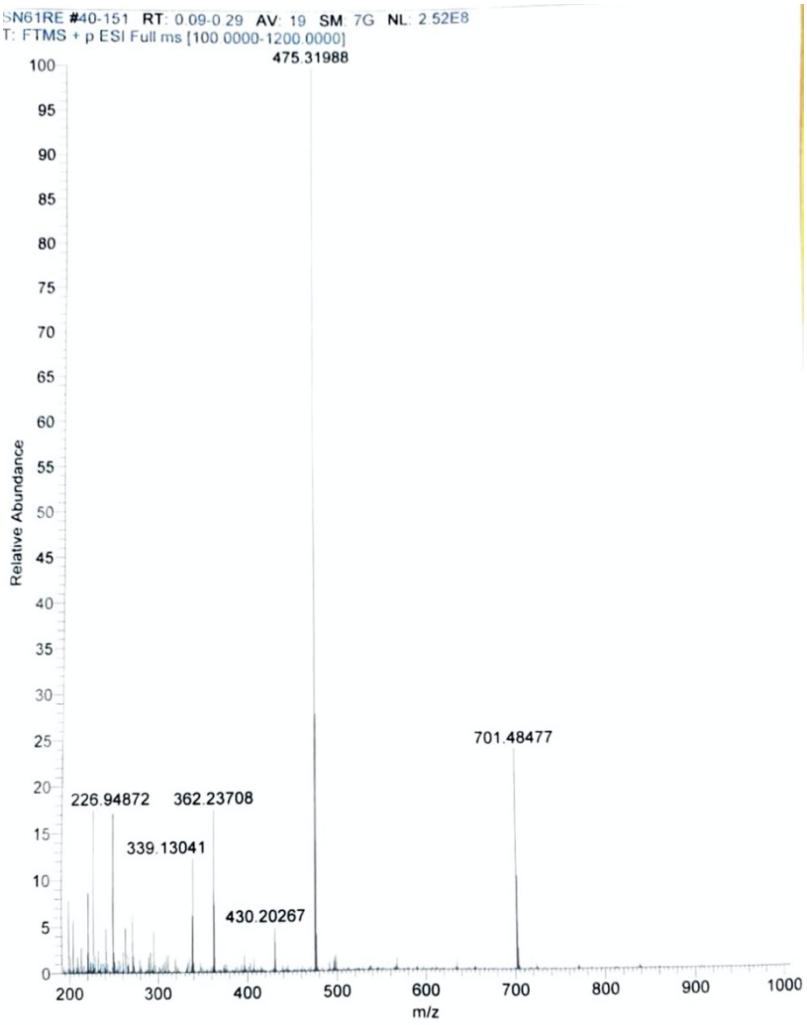

Figure S25. HRMS spectra of Re-**VI** adduct.

Table S4. The calculated and observed mass from HRMS spectra of plausible Re-**VI** adduct.

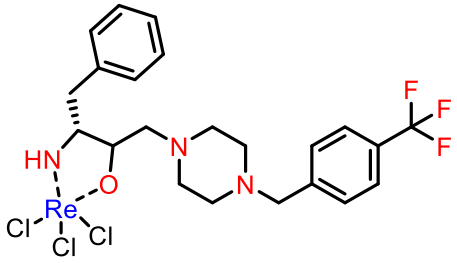 Chemical Formula: $C_{22}H_{26}Cl_3F_3N_3ORe$ m/z: 697.0651 (100.0%), 699.0622 (95.9%),	Found: 701.48477

References

1. J. R. Dilworth and S. J. Parrott, *Chem. Soc. Rev.*, 1998, **27**, 43-55.